NASA TECHNICAL MEMORANDUM

NASA TM X-68270

NASA TM X-68270

EXPERIMENTAL STRESS ANALYSIS OF LARGE PLASTIC DEFORMATIONS IN A HOLLOW SPHERE DEFORMED BY IMPACT AGAINST A CONCRETE BLOCK

by R. E. Morris
Lewis Research Center
Cleveland, Ohio 44135
July, 1973

ABSTRACT

An experimental plastic strain measurement system is presented for use on the surface of high velocity impact test models. The system was used on a hollow sphere tested in impact against a reinforced concrete block. True strains, deviatoric stresses, and true stresses were calculated from experimental measurements. The maximum strain measured in the model was small compared to the true failure strain obtained from static tensile tests of model material. This fact suggests that a much greater impact velocity would be required to cause failure of the model shell structure.

E-7577

Page Intentionally Left Blank

EXPERIMENTAL STRESS ANALYSIS OF LARGE PLASTIC DEFORMATIONS IN A HOLLOW SPHERE DEFORMED BY IMPACT AGAINST A CONCRETE BLOCK

by R. E. Morris

Lewis Research Center

SUMMARY

A hollow spherical model of a containment vessel was gaged, tested, and analyzed. The model was 0.64 m in diameter with a 1.59 cm wall thickness of stainless steel Type 304. The test velocity was 119 m/sec and the impact was against a reinforced concrete block. Impact forces greater than 15 000 times the force of gravity deformed the model without cracking or rupturing the wall of the vessel.

Experimental strain measurements were obtained on the surface of the model. Orthogonal gage lines were established on the surface of the model before the test. Gage lines were oriented parallel and perpendicular to the principal lines of symmetry of the deformations generated during impact. Procedures are presented for the measurement and analysis of plastic strains. Sources of error were investigated.

The maximum equivalent strain observed in the model was 9.4 percent of the true failure strain for the model material and was located at the sharpest bend in the deformed model near the impact face. The low level of the experimental strain suggested that the impact test velocity was much less than the velocity required to cause failure of the model.

E-7577

INTRODUCTION

Containment vessels are designed to contain radioactive materials such as nuclear reactors, nuclear fuels, isotopes, or nuclear waste products. The integrity of the vessel must be maintained even after severe deformation resulting from an accident. The purpose of this report is to describe procedures and the results of measurements of large permanent deformations generated in a model spherical containment vessel in an impact test.

Nuclear reactors generate radioactive waste materials that must be collected and stored for thousands of years. Waste contained in spent fuel must be shipped from the reactor site to the reprocessing plant. Separated waste must be moved from the reprocessing plant to a storage location. Containment of radioactive materials is important in the launching of isotope power sources for space power applications. Future operations that may pose containment problems include the launching of packages of fission waste products to be disposed of in space, and the operation of a nuclear powered air cushion vehicle.

Radioactive materials being transported for any purpose must be safely contained even in the event of a catastrophic accident to prevent contamination of the environment. One method of containing them is to enclose the radioactive materials in a spherical containment vessel which must be capable of surviving a high velocity accident. The author's previous work (ref. 1) indicated that containment vessels could survive high velocity impacts.

A testing program was initiated to obtain experimental data on the impact survivability of containment vessels. One of the test specimens, a 0.64 m (25-in.) diameter spherical vessel, is shown in figure 1. The hollow sphere test which is the subject of this report involved the impact between the 159 kg (350 lb) sphere and a 6800 kg (15 000 lb) reinforced concrete block at 119 m/sec (392 ft/sec). Figure 2 illustrates the method of testing. A concrete block is mounted on a rocket sled. The model is mounted on a styrofoam pedestal between the sled tracks. The rocket motors drive the sled up to test velocity. After the impact the test ball is caught by the cage mounted on the front of the sled. Figure 3 shows the actual test equipment.

Impact tests conducted subsequent to the hollow sphere impact test have demonstrated that model containment vessels could survive impacts against reinforced concrete blocks at more than 305 m/sec (1000 ft/sec) (ref. 2). Although models survived the high velocity impacts, they were severely deformed. Figure 4 is a picture of the deformed hollow sphere.

One measure of the severity of the deformation is to measure the plastic strain in the vessel wall and then to compare that to the ultimate strain obtained from dynamic tensile tests of specimens machined from the same material. The model containment vessel would be judged safe if the maximum strains in the model after an impact test were less than some selected fraction of the ultimate strain characteristic of the model material. If the total strain in the metal shell approaches the ultimate strain for the shell material, failure of the shell could result, followed by the release of the radioactive contents. Safety requires that this condition must be avoided.

Computer codes such as PISCES (ref. 3) and TOODY II (ref. 4) have been developed to solve dynamic impact problems in connection with military missile design and missile penetration problems. Computer solutions have been obtained for impact deformation problems. A method was needed for obtaining experimental deformation data to verify the computer analysis by comparing the theoretical computer output with the experimental data.

None of the many strain measurement instruments available could survive the tremendous impact forces to provide data on the large strains generated in the spherical shell of the model during impact. Some method was needed to measure the large strains and thus determine whether the shell of the model had been strained severely relative to the ultimate strain for the shell material.

The procedures for the experimental measurement and analysis of large plastic strains and stresses presented herein were developed to solve these problems. The assumptions delineated provide limitations for this stress and strain measurement method.

SYMBOLS

E nominal plastic strain, cm/cm

G rise gage length, cm

g gravitational acceleration, m/sec^2

K strength coefficient, N/cm^2

L gage line surface length, cm

L' gage line surface length after deformation, cm

n strain hardening exponent

R surface radius, cm

X chord length, cm

Y rise measurement, cm

ε true strain, $Ln(1 + E)$, cm/cm

ε_0 equivalent strain by the distortion energy theory, cm/cm

σ true stress, N/cm^2

σ' deviatoric stress, N/cm^2

σ_0 equivalent stress by the distortion energy theory, N/cm^2

ANALYSIS

Two perpendicular gage lines are established on the surface of the model. The lines are parallel to the principal axes of stress and plastic strain to be generated during deformation. The lengths of the gage lines are measured before and after deformation.

The length of a gage line is found by measuring the chordal length between the extremities of the line and the rise length which is the distance from the center of the chord to the surface of the sphere.

Figure 5 shows the geometry of gage line measurement. Solving for

the radius, R, in triangle OAB we have

$$R = \frac{G^2}{8Y} + \frac{Y}{2} \tag{1}$$

where G is the chord length, and Y is the rise measurement.

The following list of assumptions are required for the analysis of plastic strains and stresses in the surface of the model containment vessel.

1. The material is isotropic.

2. Elastic strains are neglected.

3. The state of plastic strain is uniform throughout the surface element where measurements are taken.

4. Orthogonal principal axes of stress and plastic strain coincide.

5. One principal axis of the orthogonal set of stress-strain axes is normal to the surface of the element during deformation.

6. Plastic strains are proportional to and have directions parallel to the lines of action of the stresses acting.

7. Straight lines remain straight after straining.

8. Plastic strains result from monotonically increasing or decreasing equivalent stress.

9. Radii of gage lines on the surface of the sphere are uniform over the length of each gage line before and after straining.

10. Equivalent stress and strain associated with plastic flow in the element are given by the distortion energy theory.

Nominal strain, E, on a given gage line is obtained from

$$E = (L' - L)/L \tag{2}$$

where L is the original surface length of a gage line and L' is the surface length after deformation.

Volume is constant during plastic deformation. Let E_1, E_2, and E_3 be the orthogonal principal nominal strains on the surface of the model. Then the volume of a unit cube with sides parallel to the principal axes before and after deformation must be equal to one.

$$(1 + E_1)(1 + E_2)(1 + E_3) = 1 \tag{3}$$

If E_1 and E_2 are measured biaxial principal plastic strains in the surface of the model, then E_3 is given by equation (3). Taking the logarithm of both sides of equation (3) yields

$$\varepsilon_1 + \varepsilon_2 + \varepsilon_3 = 0 \tag{4}$$

where ε_i are the true principal plastic strains.

The equation for the equivalent strain, ε_0, according to the distortion energy theory is a function of the true principal plastic strains.

$$\varepsilon_0 = \frac{\sqrt{2}}{3}\left[(\varepsilon_1 - \varepsilon_2)^2 + (\varepsilon_2 - \varepsilon_3)^2 + (\varepsilon_3 - \varepsilon_1)^2\right]^{1/2} \tag{5}$$

The true equivalent strain is related to stress in the exponential equation

$$\varepsilon_0 = K\sigma_0^n \tag{6}$$

In this equation K is the strength coefficient and n is the strain hardening exponent. Variables K and n are evaluated by correlating the equation with true stress-strain tensile test data.

Deviatoric true stresses are identified with primes. The sum of three principal deviatoric stresses is zero.

$$\sigma_1' + \sigma_2' + \sigma_3' = 0 \tag{7}$$

Plastic flow equations are given by Faupel (ref. 5).

$$\varepsilon_1 = \frac{\varepsilon_0}{\sigma_0}\left[\sigma_1 - \frac{1}{2}(\sigma_2 + \sigma_3)\right] \tag{8}$$

$$\varepsilon_2 = \frac{\varepsilon_0}{\sigma_0}\left[\sigma_2 - \frac{1}{2}(\sigma_1 + \sigma_3)\right] \tag{9}$$

$$\varepsilon_3 = \frac{\varepsilon_0}{\sigma_0}\left[\sigma_3 - \frac{1}{2}(\sigma_1 + \sigma_2)\right] \tag{10}$$

These equations also hold for the deviatoric stresses. Combining equations (7) to (10) yields

$$\sigma_1' = \frac{2}{3}\frac{\sigma_0}{\varepsilon_0}\varepsilon_1 \tag{11}$$

$$\sigma_2' = \frac{2}{3}\frac{\sigma_0}{\varepsilon_0}\varepsilon_2 \tag{12}$$

$$\sigma_3' = \frac{2}{3}\frac{\sigma_0}{\varepsilon_0}\varepsilon_3 \tag{13}$$

In the event that one of the principal stresses is zero, such as at a free surface, then the true principal stresses can be found. Let $\sigma_3 = 0$. Then

$$\sigma_1 = \sigma_1' - \sigma_3' \tag{14}$$

$$\sigma_2 = \sigma_2' - \sigma_3' \tag{15}$$

$$\sigma_3 = \sigma_3' - \sigma_3' = 0 \tag{16}$$

This completes the equations required for the analysis of the plastic strain data.

PROCEDURE

Fabrication and Testing

The model containment vessel was fabricated at NASA Lewis Research Center. Two hemispherical heads were joined with a circumferential weld. Gage lines were established on the surface of the sphere and pretest measurements were recorded. Figure 1 shows a model prepared for testing.

The impact test was conducted at the Sandia Sled Track, Albuquerque, N.M. as described in reference 6. The model survived the impact test (see fig. 4). No cracks or fractures in the spherical shell were found in a helium leak test or in a visual inspection of the deformed model. The impact test velocity was 119 m/sec (392 ft/sec).

Impact forces were evaluated in two ways. An accelerometer was mounted on the model opposite to the impact face, and high speed motion pictures of the impact were taken. The 15 000 g range of the accelerometer was exceeded. Analysis of photographs taken at speeds of 7000 and 14 000 frames per second provided an average acceleration rate of 15 000 g for the impact.

Upon completion of the impact test the model was returned to LeRC for the analysis of the experimental strain measurements. Important test data is listed in table I.

Location of Gage Lines

Gage lengths were established on the surface of the model in square arrays by locating punch marks at the corners of two-inch squares as shown in figure 1. The centers of the gage line arrays were located according to the gage location layout shown in figure 6. The top view shows the meridional centerlines spaced 45° apart. The front and side views show the latitudinal centerlines spaced at 30° intervals. The θ and ϕ directions are indicated in the top and side views.

Figure 7 shows an array of punch marks at position F2. Two of the gage lines are parallel to and spaced 2.54 cm (1.0 in.) on either side of the number 2 centerline of latitude. The other two gage lines in the square array are parallel to, on opposite sides of, and spaced 2.54 cm (1.0 in.) from the meridional centerline F.

Strain Measurement

Plastic strains were obtained by measuring the surface distance between a pair of punch marks before and after the impact. The surface distance was calculated from a measurement of the chord length between punch marks and the measurement of the rise of the surface.

The dial caliper shown in figure 8 was used to measure the chordal distance between punch marks. In the same figure, the dial indicator assembled in the rigid steel frame is called a rise gage. This instrument was used to measure the rise of the surface between each pair of punch marks. The gage is set to zero on a surface plate. The dial indicator then gives a rise reading when placed on a curved surface. The gage length is the fixed distance between the arms of the frame. The gage length of the large frame shown separately is 6.350 cm (2.500 in.). The frame in the assembled rise gage has a gage length of 3.175 cm (1.250 in.). The small frame was used only for surfaces with radii less than 10 cm. The larger frame was used on surfaces with radii greater than 10 cm.

Rise and chord measurements were taken before and after impact. Radii were obtained from rise gage data using equation (1). The length of gage lines were calculated before and after impact using

$$L = 2R \sin^{-1}(X/2R) \tag{17}$$

Then nominal strains were obtained using equation (2).

Radii calculated were used to plot the geometry of the deformed model. Figure 9 is a plot of surface radius against position on a meridian. Figure 10 shows the geometry of the deformed model based on the radius and other physical measurements. The graph of sphere geometry and the graph of E_{θ} against position were used to establish slopes

of the E_θ graph at the center position for each square array of gage lines. Corrections were then calculated for E_θ at the extremities of each E_θ gage line using the graphically measured slopes and assuming a linear variation of E_θ over the length of the gage line.

Mutually perpendicular strains E_θ and E_ϕ were calculated for each E_ϕ gage line position on the curved surface. The third nominal plastic principal strain normal to the surface was found from the constant volume relation equation (3). The true plastic strains were obtained by taking the natural logarithm of one plus the nominal principal plastic strain for each of the three orthogonal principal strains. Then the equivalent strains were calculated using equation (5).

Stress Calculations

The constants in equation (6) were evaluated using experimental data for the yield strength, the ultimate strength, and the ultimate strain for the model material from table I. Equation (6) provided an equivalent stress value for each calculated value of equivalent strain. Deviatoric stresses associated with the deformation were found using equations (11) to (13). The true principal stresses associated with the plastic deformation were found for principal stresses at a free surface by subtracting the deviatoric stress normal to the free surface from each of the orthogonal stresses at each position using equations (14) to (16).

RESULTS AND DISCUSSION

The hollow spherical model containment vessel was fabricated at Lewis Research Center, tested by impact against a concrete block at Sandia Sled Track, and returned to LeRC for measurement and analysis. Plastic strains were measured, graphed, and related to stresses in the model. This discussion covers the properties of the sphere material, the strain measurements, stress calculations, and an error analysis of the methods of measurement. Preliminary results of the hollow sphere impact test are described in reference 6. Important test data is listed in table I.

Material Properties

Properties of the sphere material were obtained from static tensile tests of specimens machined from coupons cut from parent metal in the relatively undeformed head of an impact model after testing. Although dynamic tests were desired, static tests were conducted since dynamic test equipment was not available. One specimen was oriented perpendicular to the circumferential weld in the model. The second specimen was oriented parallel to the weld. Average data from the two specimens is listed in table I.

The stress-strain diagram needed to convert true strains into true stresses was based on reference 7 and data listed in table I. The yield strength was assumed to be equal to the true stress at yield. The nominal strain at ultimate strength was 0.60 cm/cm from reference 7. The true ultimate strain of 0.47 cm/cm was calculated using the nominal value of ultimate strain. The true ultimate stress of 101 000 N/cm^2 (146 400 psi) was obtained from the nominal ultimate strain and the average ultimate stress in the table. The average true failure strain of 130 percent was based on the average reduction in area of the test specimens. The equation for the stress-strain curve was found by evaluating the constants in the exponential equation

$$\sigma_0 = K\varepsilon_0^n \tag{6}$$

K was found to be 118 136 N/cm^2 (171 340 psi) and the exponent $n = 0.20746$ provided the slope of the equation on the log-log plot in figure 11.

Strain Measurements

Gage lines had a nominal two-inch gage length. Consequently plastic deformations measured represented average strains over the two-inch gage lengths. Strain measurements in the ϕ-direction (see fig. 6) were probably uniform over the gage length and hence were representative of the strain in the surface of the model. Strain measurements in the θ-direction were averages of strains that generally varied over the gage length. Strains in the θ direction were corrected for variations as described in the Procedures section.

Figures 9 and 10 show radius variations along the surface meridian studied. The edges of the hemispheres were thicker than the nominal 15.88 mm (0.625 in.) as a result of deformations caused when the heads were die-formed. The heads were assembled with a reinforced through-weld. These factors caused the spherical surface to be stiffer in the circumferential weld area.

The short radius at the 38.1 cm (15 in.) position in figure 9 corresponds with the bulge at the corresponding position in figure 10. The centerline of the weld is at the 50.5 cm (19.87 in.) position. As the shell was pushed outward from the line of symmetry below the weld, flexure occurred in the weld area and the radius became negative as shown in figure 9. Figure 12 corresponds with the geometry data, and ε_θ is negative at the weld. At about 55.9 cm (22 in.) another flexure occurred and the radius returned to positive values. Figure 12 indicates the position of flexure as ε_θ goes from negative to positive at that position on the shell. The minimum radius was found at 63.5 cm (25 in.). The maximum strain in the ε_θ direction in figure 12 corresponds with the location of the minimum radius shown in figures 9 and 10. Thus the experimental radius data and the average ε_θ strains calculated from the experimental chord and rise measurements were used to establish the ε_θ

curve in figure 12. Slopes measured on the curve were used to correct ε_θ so that strain calculations could be made for each ε_ϕ measurement. The maximum equivalent strain was found to be 12.2 percent at the minimum radius position. From table I, the average true strain obtained from the reduction in area of tensile test specimens was 130 percent. The maximum measured equivalent strain was, therefore, 9.4 percent of the true failure strain for the model material. The fact that the maximum measured equivalent strain was such a small percentage of the true failure strain suggests that the test velocity of the hollow sphere impact test was well below the impact test velocity required to cause failure of the model shell structure.

Calculated Stresses

The strains plotted in figure 12 were used with equations (6), and (11) to (16) to obtain the stresses plotted in figures 13 and 14. Both figures show that the principal stresses in the surface of the relatively undeformed half of the model were compressive.

The deviatoric stresses are plotted in figure 13. The radial stress σ_r' is positive down to the weld. Then the stress turns sharply negative, or compressive. The stress σ_ϕ' is negative around the head from the coupling to the weld, and then turns positive. The section of σ_ϕ'-stresses which are tensile in figure 13 corresponds with the section of the shell which was bulged out past the original shell radius as shown in figure 10. Around the shell past the minimum radius towards the impact face, the σ_ϕ'-stress turns compressive again. The σ_θ-stress also corresponds with the bends and flexures in the shell. Figures 9 and 10 show a negative radius at the weld. This deformation corresponds with compressive σ_θ'-stresses. At the minimum radius, the sharp bend in the shell corresponds with tensile values for σ_θ'.

The equivalent stresses are the same in figures 13 and 14. Stresses are moderate in the undeformed half of the shell. Values are higher at the weld and the maximum value is at the sharp bend with the minimum radius. The dip in the equivalent stress shown on the graph between the weld and the minimum radius corresponds with an inflection in the shell as the radius turns from negative to positive (see fig. 9). The maximum value of equivalent stress is 76 500 N/cm^2 (111 000 psi) at the minimum radius.

Figure 14 results from the assumption that the radial stress normal to the surface of the shell is zero. This assumption is probably not valid beyond the minimum radius towards the impact face. The graph reveals that the principal biaxial stresses in the undeformed half of the model are definitely compressive. A sharp transition occurs below the weld towards the impact face. At the position of the maximum stress the biaxial stresses are essentially equal tensile stresses.

Analysis of Errors in Strain Measurements

The impact test deformed the model. A minimum surface radius of 4.65 cm measured on the deformed model compared with a nominal surface radius of 32.1 cm before the test. Punch marks used to define the extremities of gage lines were rotated and deformed by strains in the metal surface. Changes in surface radii and the deformation of punch marks increased the error in post-test measurements.

Errors in measurement varied with the level of strain being measured. Strains less than 0.1 percent could not be detected. Accuracy of measurement increased as the level of strain increased. Two experimental measurements are required to determine the length of a gage line before deformation. Two more measurements are needed to obtain the deformed length. The total error in a strain measurement is the sum of the errors in the pre-test and post-test measurements. Errors were analyzed for two levels of strain: one percent, and ten percent. Results of the analysis are listed in table II.

The rise gage measurement determined the surface radius which was assumed to be uniform over the gage length of the instrument. All pre-test measurements were taken with the rise gage using the frame having the 6.35 cm (2.50 in.) gage length. The gage was read to the nearest 25 μm (0.001 in.). The maximum error of ±13 μm (0.0005 in.) in a gage reading was associated with an error of 0.2 percent apparent strain in the measurement of 1 percent nominal principal strain. The corresponding error in the measurement of 10 percent strain was negligible.

A dial caliper with a least count of 25 μm (0.001 in.) was used to measure chord lengths between punch marks at the extremities of gage lines. The uncertainty in a caliper reading of ±13 μm (0.0005 in.) was equivalent to an error of ±2.5 percent at the 1 percent strain level and 0.3 percent at the 10 percent level of strain. This source of error is the same for both pre-test and post-test measurements.

Post-test rise gage measurements had the greatest error at the minimum radius. Errors were generally greater when the small 3.175 cm (1.250 in.) frame was used in the rise gage. Error at the minimum radius was 5.6 percent at the 1 percent strain level and 0.6 percent at the 10 percent level as shown in table II.

Punch mark deformation and rotation made a contribution of error in post-test measurement. Punch marks were elongated in the direction of the principal nominal strain. Centerlines of punch marks also rotated as the surface radius changed during deformation. Both factors could affect the fit of the caliper points in the punch marks resulting in apparent strain. A graphical estimate of error showed that 2.0 percent error could result from this source at the 1 percent level of strain. At the ten percent level, punch mark deformation was increased but the percentage error was the same.

The final source of error considered involved the gage line orientation with respect to the principal axis of strain in the model. An experimental measurement contains error when the gage line and the principal axis of strain are not parallel. The error in a principal strain measurement was investigated for the case of a 5^{o} misalinement of gage line and principal strain axis. When the principal nominal strain was 1 percent, the experimental measurement was in error by 1.1 percent. The error in the measurement of 10 percent nominal strain was 1.0 percent.

As previously mentioned the maximum error in a strain measurement occurs when each error component acts to increase the total error. Adding the components for the 1 percent level of strain yields a maximum error of 14 percent. The maximum error in the measurement of 10 percent strain amounts to 4 percent.

CONCLUDING REMARKS

Experimental measurements of plastic strain were made on the surface of a spherical Type 304 stainless steel model deformed by impact which caused acceleration forces greater than 15 000 g's. Strains were measured by establishing gage lines on the surface of the model and measuring the difference in the lengths of lines before and after impact deformation of the model.

Static tensile tests of two perpendicular specimens cut from model material were conducted. Average mechanical properties were used to obtain a true stress-strain correlation for the model material. The average reduction in area provided a true failure strain of 130 percent.

Analysis of errors in the measurement of 1 percent nominal strain gave a total maximum error of 14 percent. The total maximum error in the measurement of 10 percent nominal strain was 4 percent.

The maximum distortion energy equivalent strain of 12.2 percent was measured at the sharpest bend in the surface of the deformed model. The maximum strain measured on the model was 9.4 percent of the true failure strain obtained from static tensile tests of model material. This fact suggests that a much greater impact velocity would be required to cause failure of the model.

REFERENCES

1. Morris, Richard E.: Empirical Correlation of Small Hollow Sphere Impact Failure Data Using Dimensional Analysis. NASA TM X-52874, 1970.

2. Puthoff, Richard L.: Richard L.: A 1055 Ft/sec Impact Test of a Two Foot Diameter Model Nuclear Reactor Containment System Without Fracture. NASA TM X-68103, 1972.

3. Hofmann, Ronald; Hancock, S. L.; Puthoff, R. L.; and Wohl, M.: Computed Response of Spherical Shielding to Impact Loading. Rep. TCAM Tech. Memo 72-7, Appl. Mech. Dept., Physics International Co., May 1972.

4. Bertholf, L. D.; and Benzley, S. E.: TODDY II - A Computer Program for Two-Dimensional Wave Propagation. Rep. SC-RR-68-41 Sandia Lab., Nov. 1968.

5. Faupel, Joseph H.: Engineering Design. Johy Wiley & Sons, Inc., 1964.

6. Puthoff, R. L.; and Dallas, T.: Preliminary Results on 400 ft/sec Impact Tests of Two 2-foot Diameter Containment Models for Mobile Nuclear Reactors. NASA TM X-52915, 1970.

7. Wolf, J.; and Brown, W. F. Jr., eds.: Aerospace Structural Metals Handbook. Vol. 1: Ferrous Alloys. The Mechanical Properties Data Center (AFML-TR-68-115), Mar. 1967.

TABLE I. - TEST DATA

Sphere		
Outside diameter	64.3 cm	25.3 in.
Wall thickness, (nom.)	15.9 mm	5/8 in.
Weight	159 kg	350 lb
Material	Type 304 stainless steel	
Block		
Material	Steel-reinforced concrete	
Dimensions	1.37 m cube	4-1/2 ft cube
Weight	6800 kg	15 000 lb
Impact data		
Velocity at impact	119 m/sec	392 ft/sec
Average acceleration	15 000 g	15 000 g
Peak acceleration	Greater than 15 000 g of instrumentation	
Sphere material properties		
0.2 percent yield strength	32 500 N/cm^2	47 200 psi
Nom. ultimate tensile strength	64 100 N/cm^2	91 500 psi
True ultimate stress	101 000 N/cm^2	146 500 psi
Elongation in 2.54 cm, percent	72	
Reduction in area, percent	72.6	
True ultimate strain, percent	47	
True failure strain, percent	130	

TABLE II. - ERRORS IN PLASTIC STRAIN MEASUREMENT

Level of plastic strain (percent)	1	10
Pre-test measurements		
Rise gage error (R = 32.1 cm nom.)	0.2	0.0
Dial caliper	2.5	0.3
Post-test measurements		
Rise gage error ($R \geq 4.65$ cm)	5.6	0.6
Dial caliper	2.5	0.3
Punch mark deformation	2.0	2.0
Gage line orientation with principal strain axis ($\pm 5^{o}$)	1.1	1.0
Total error (percent)	14	4

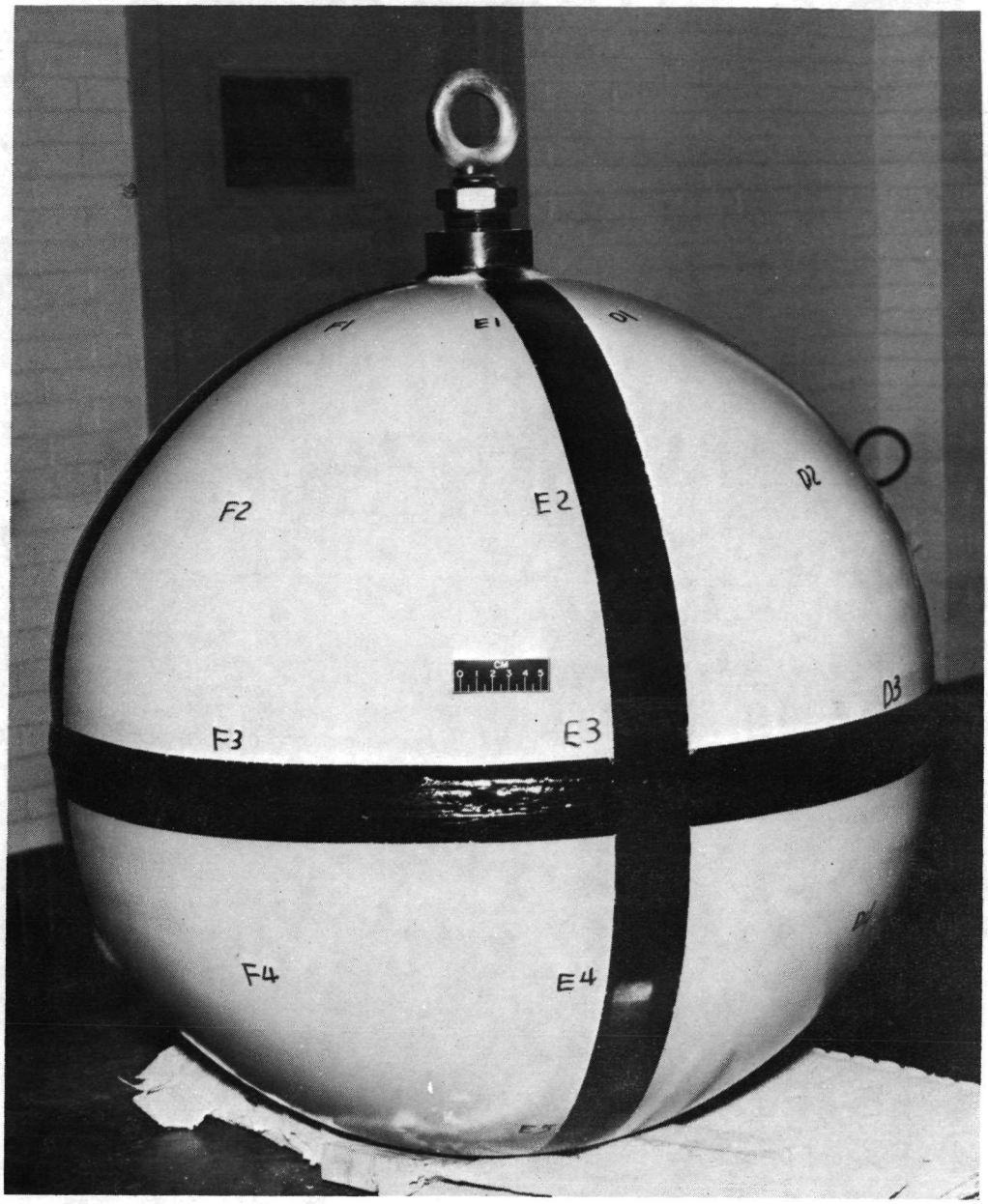

Figure 1. Impact Test Model.

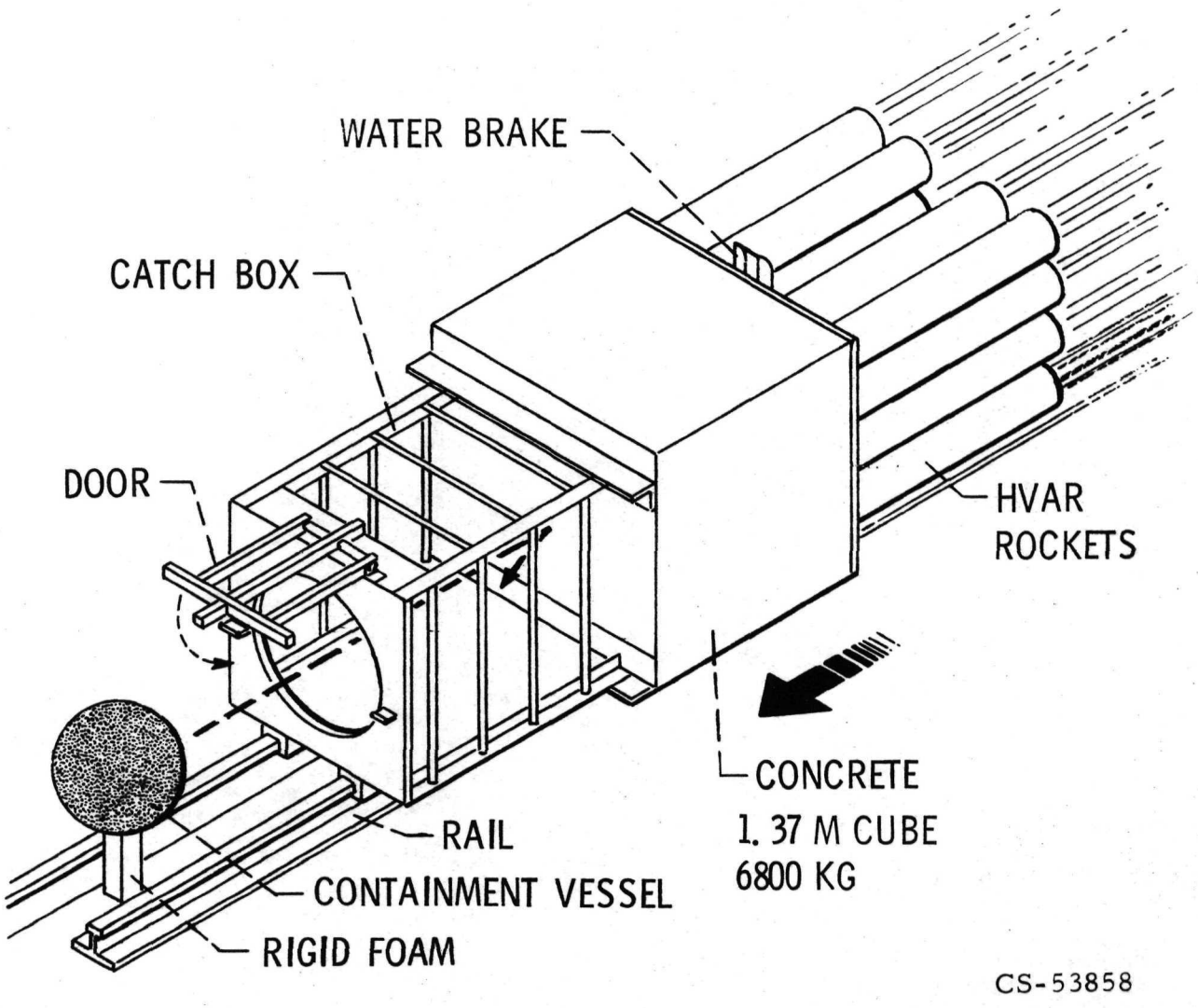

Figure 2. - Schematic of an impact test of a moving concrete block and a stationary model of a spherical reactor containment vessel.

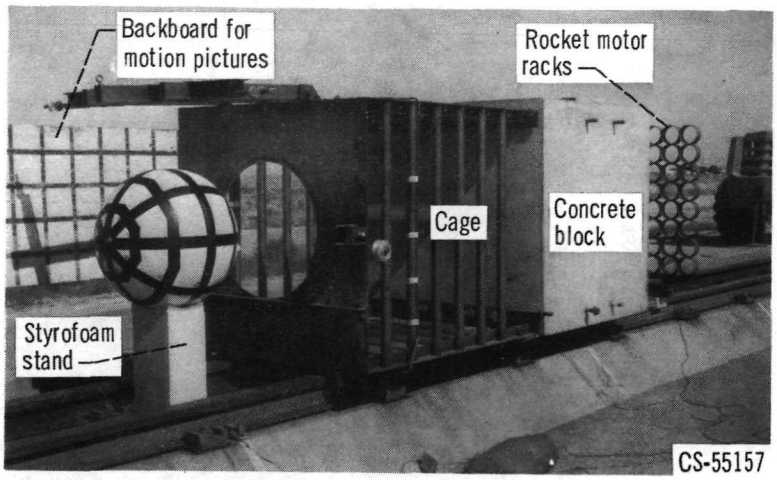

Figure 3. - Test equipment for moving block impact with a stationary model of a spherical reactor containment vessel.

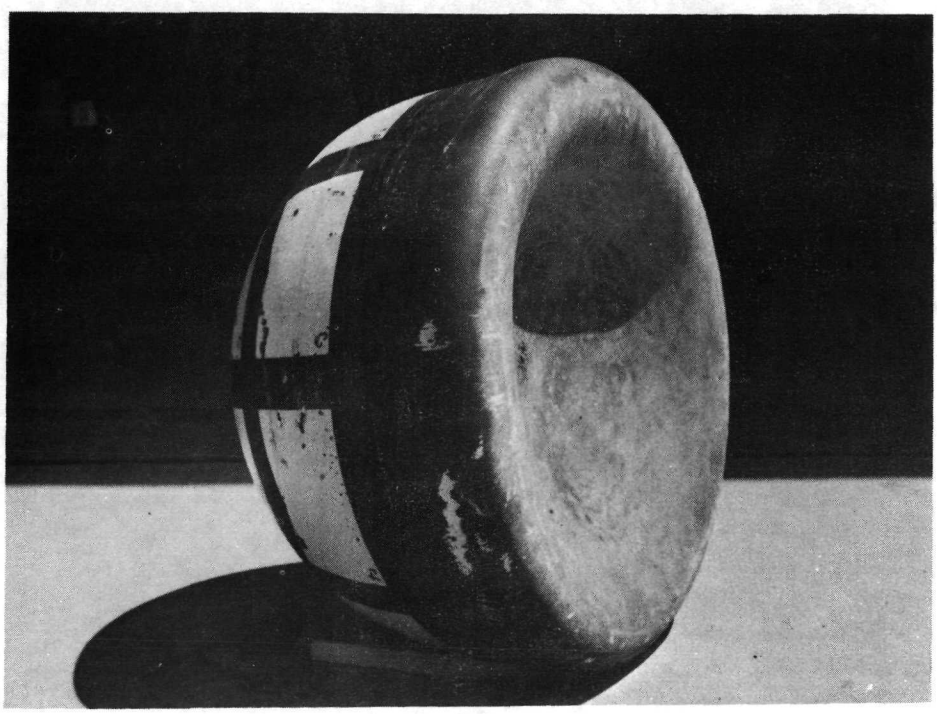

Figure 4. Hollow sphere after impact at 119 m/sec (392 ft/sec).

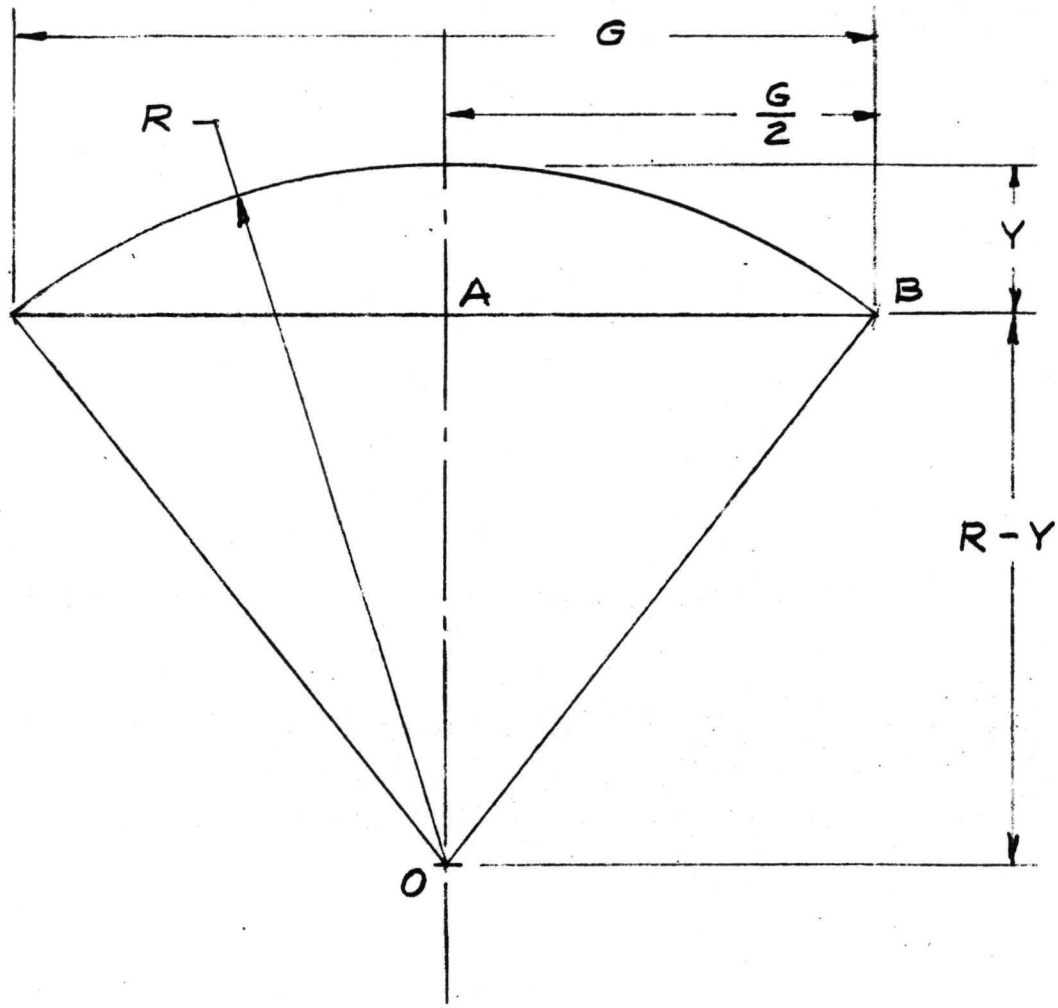

Figure 5. Geometry of gage line measurement.

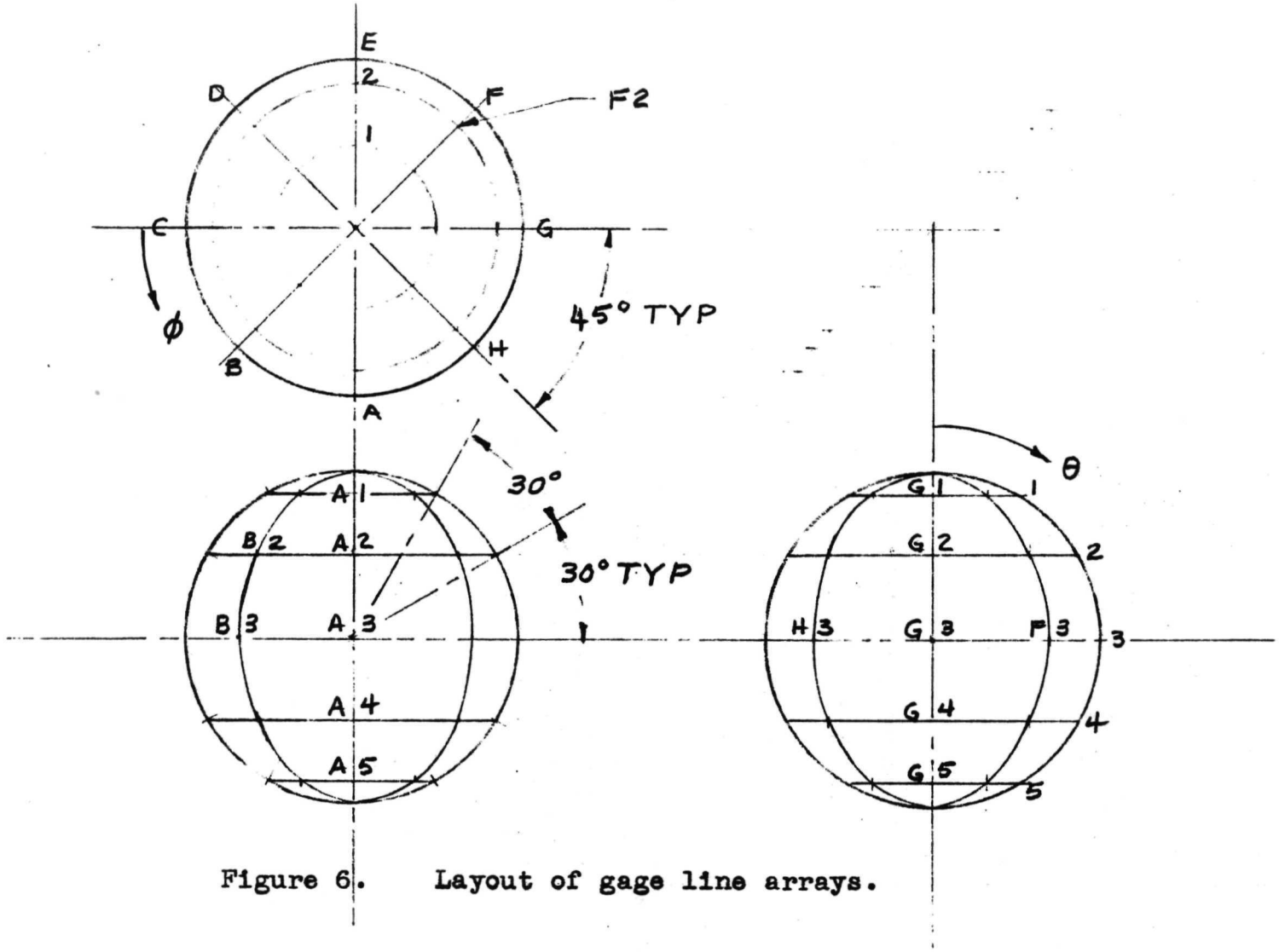

Figure 6. Layout of gage line arrays.

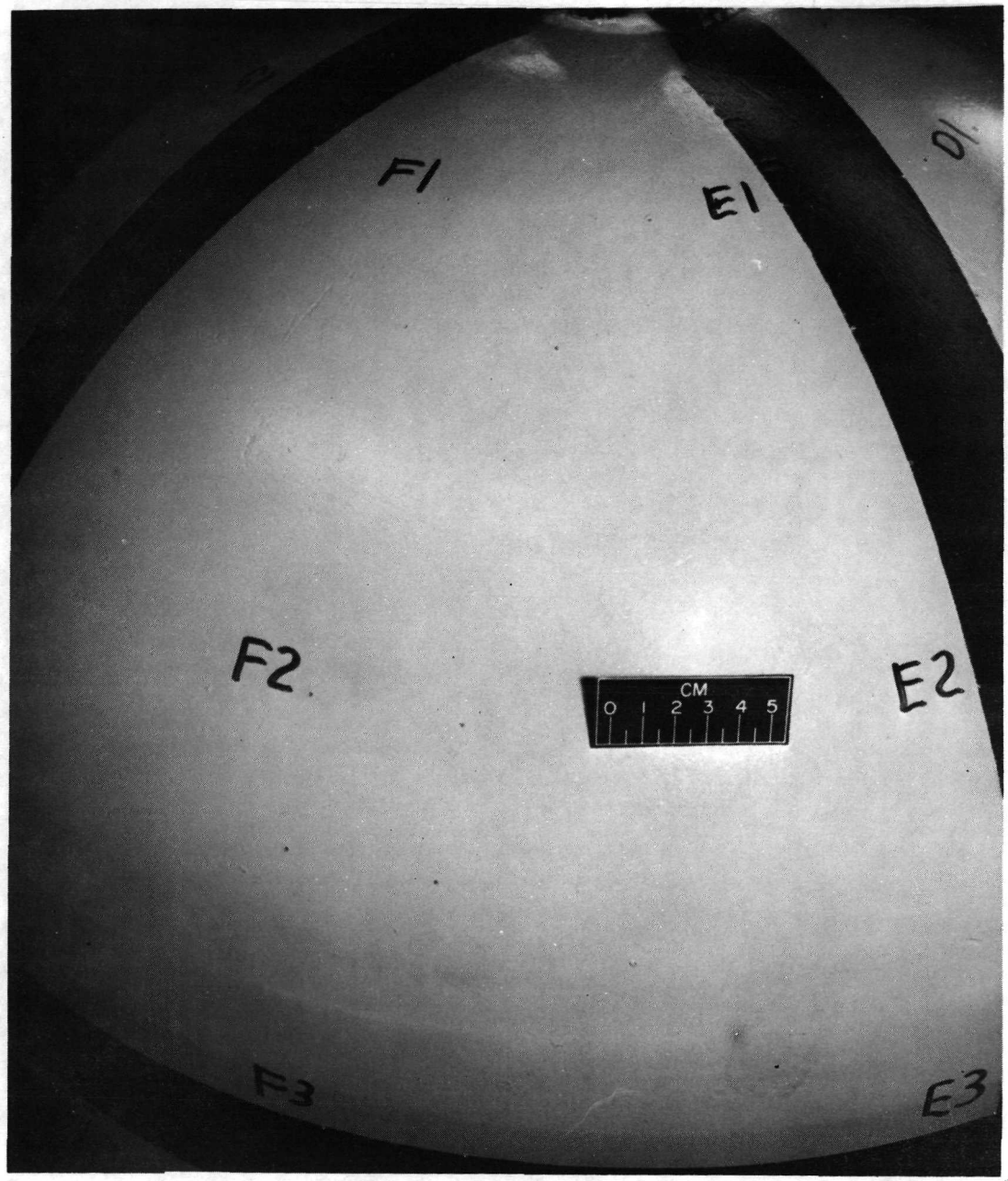

Figure 7. Square array of punch marks at position F2.

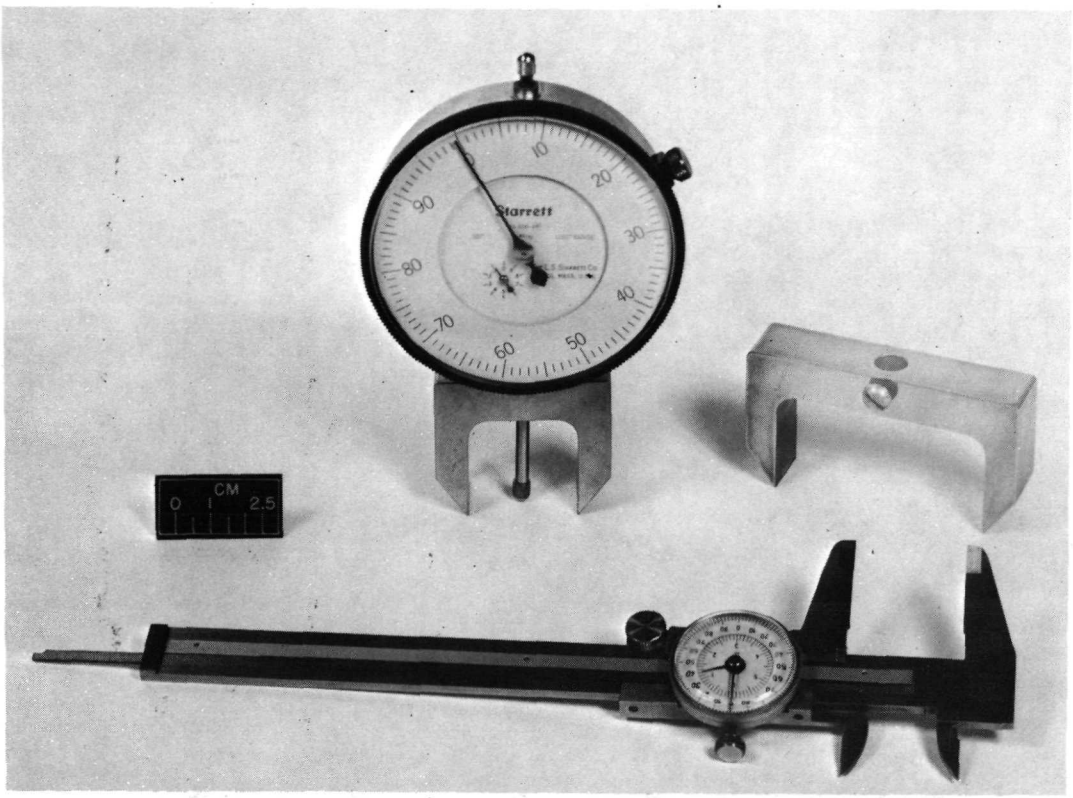

Figure 8. Rise measurement gage with 3.175 cm (1.250 in.) gage length, rise gage frame with 6.350 cm (2.500 in.) gage length, and a dial caliper used for gage line chord length measurement

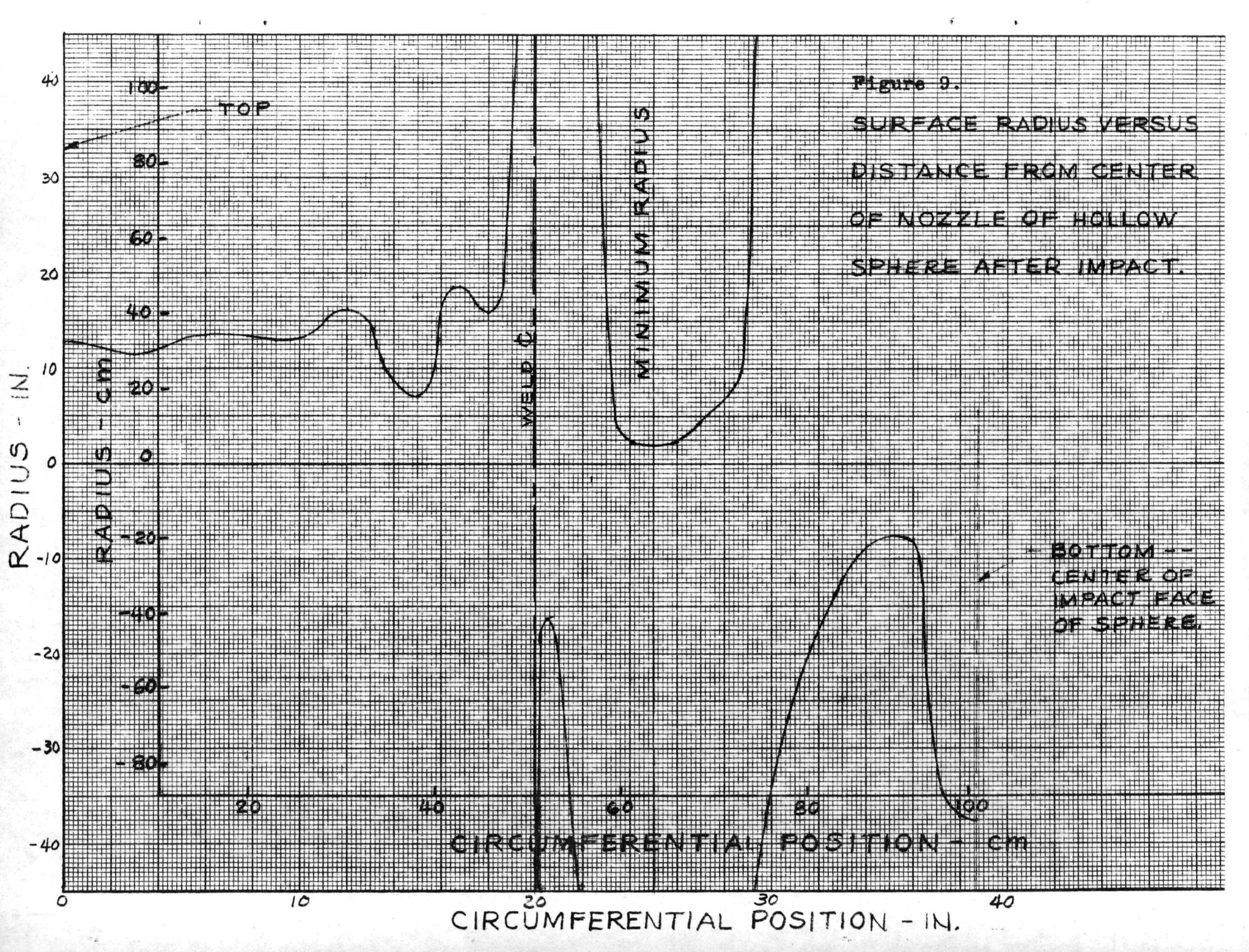
Figure 9.
SURFACE RADIUS VERSUS DISTANCE FROM CENTER OF NOZZLE OF HOLLOW SPHERE AFTER IMPACT.
TOP
WELD ℄
MINIMUM RADIUS
BOTTOM -- CENTER OF IMPACT FACE OF SPHERE.
RADIUS - cm
RADIUS - IN.
CIRCUMFERENTIAL POSITION - cm
CIRCUMFERENTIAL POSITION - IN.
100
80
60
40
20
0
-20
-40
-60
-80
40
30
20
10
0
-10
-20
-30
-40
20
40
60
80
100
0
10
20
30
40

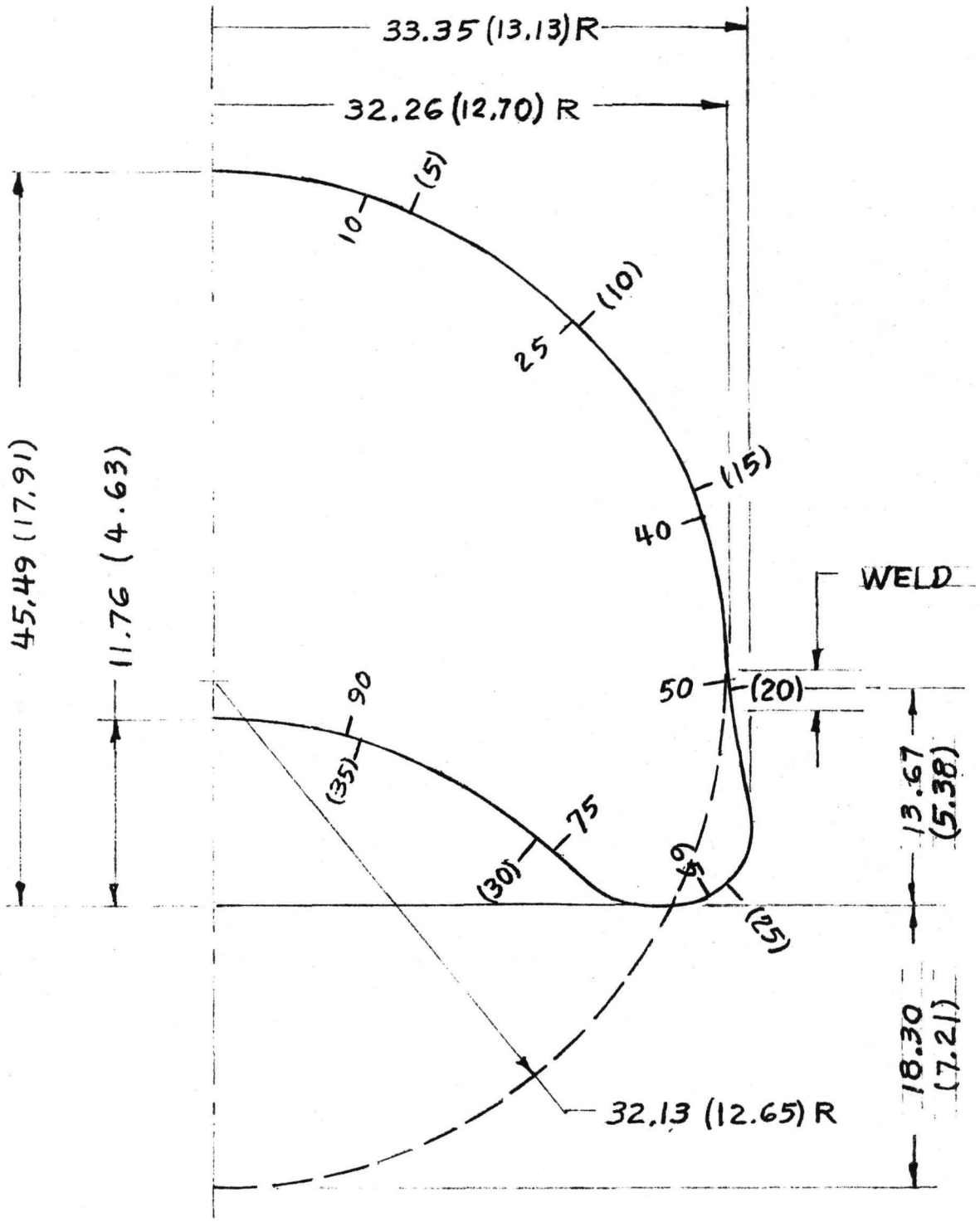

Notes: Scale - $\frac{1}{4}$ size
Dimensions in inches in parentheses
Principal dimensions - cm

Figure 10. Geometry of the deformed hollow sphere.

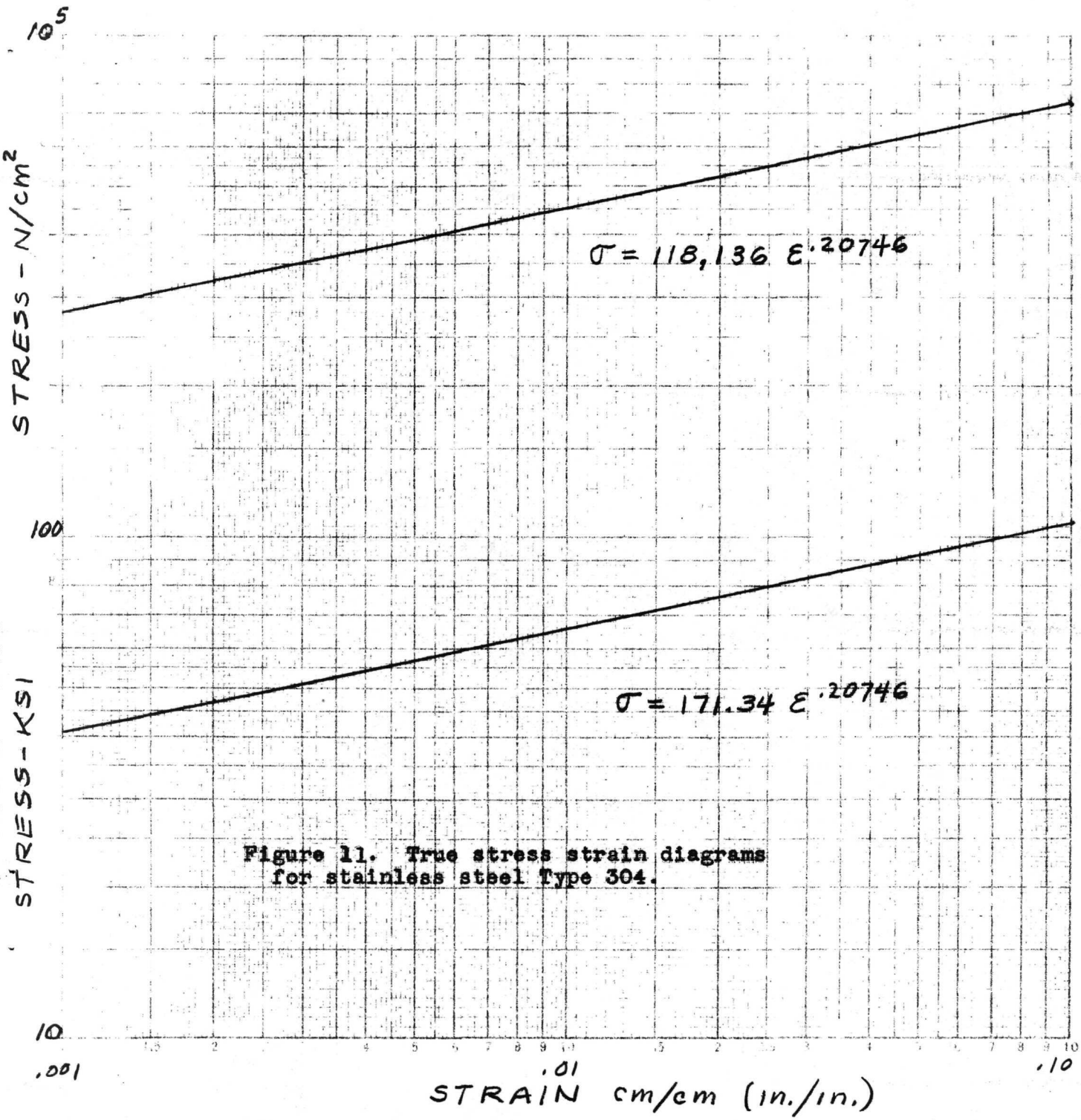

Figure 11. True stress strain diagrams for stainless steel Type 304.

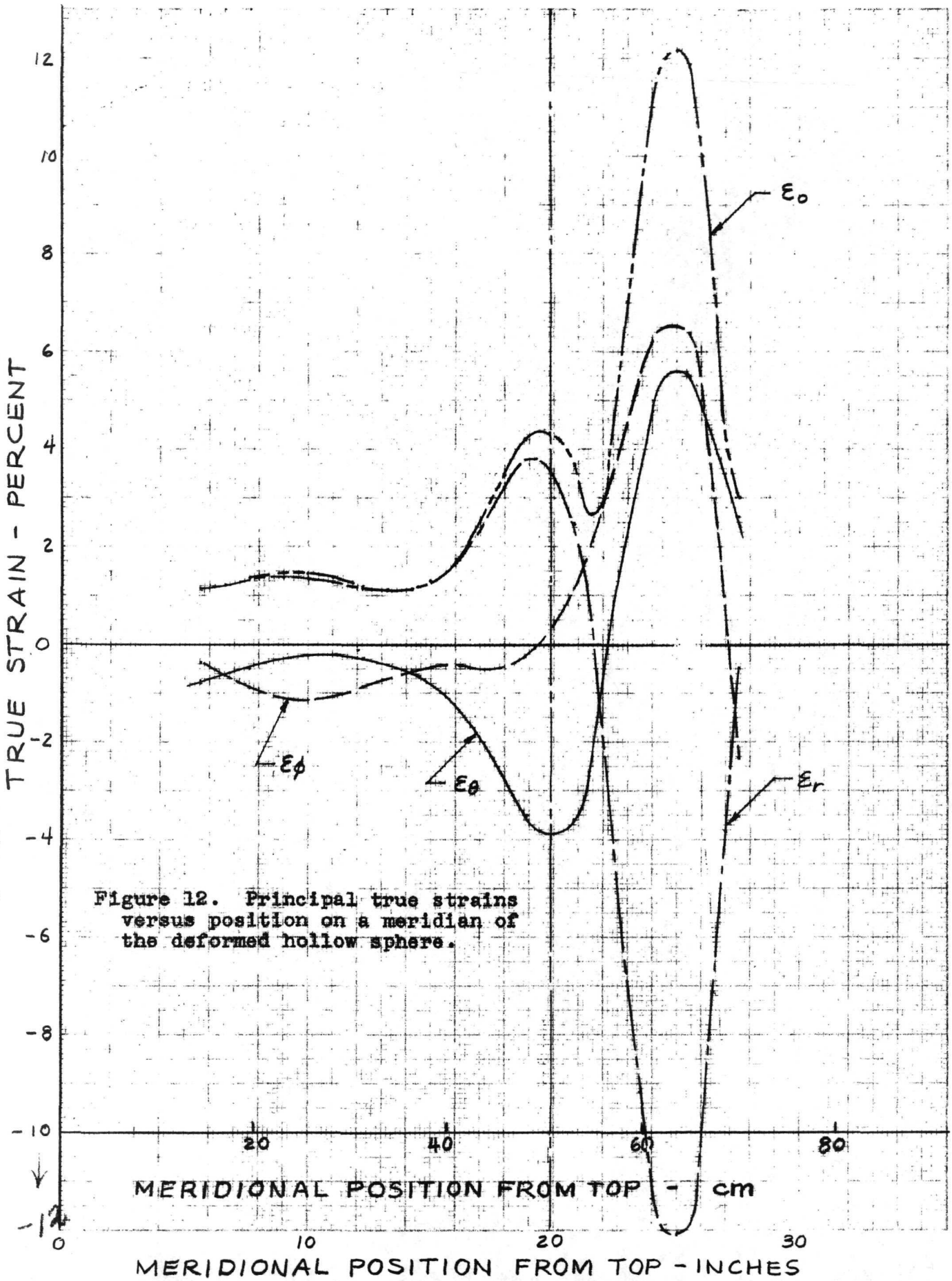

Figure 12. Principal true strains versus position on a meridian of the deformed hollow sphere.

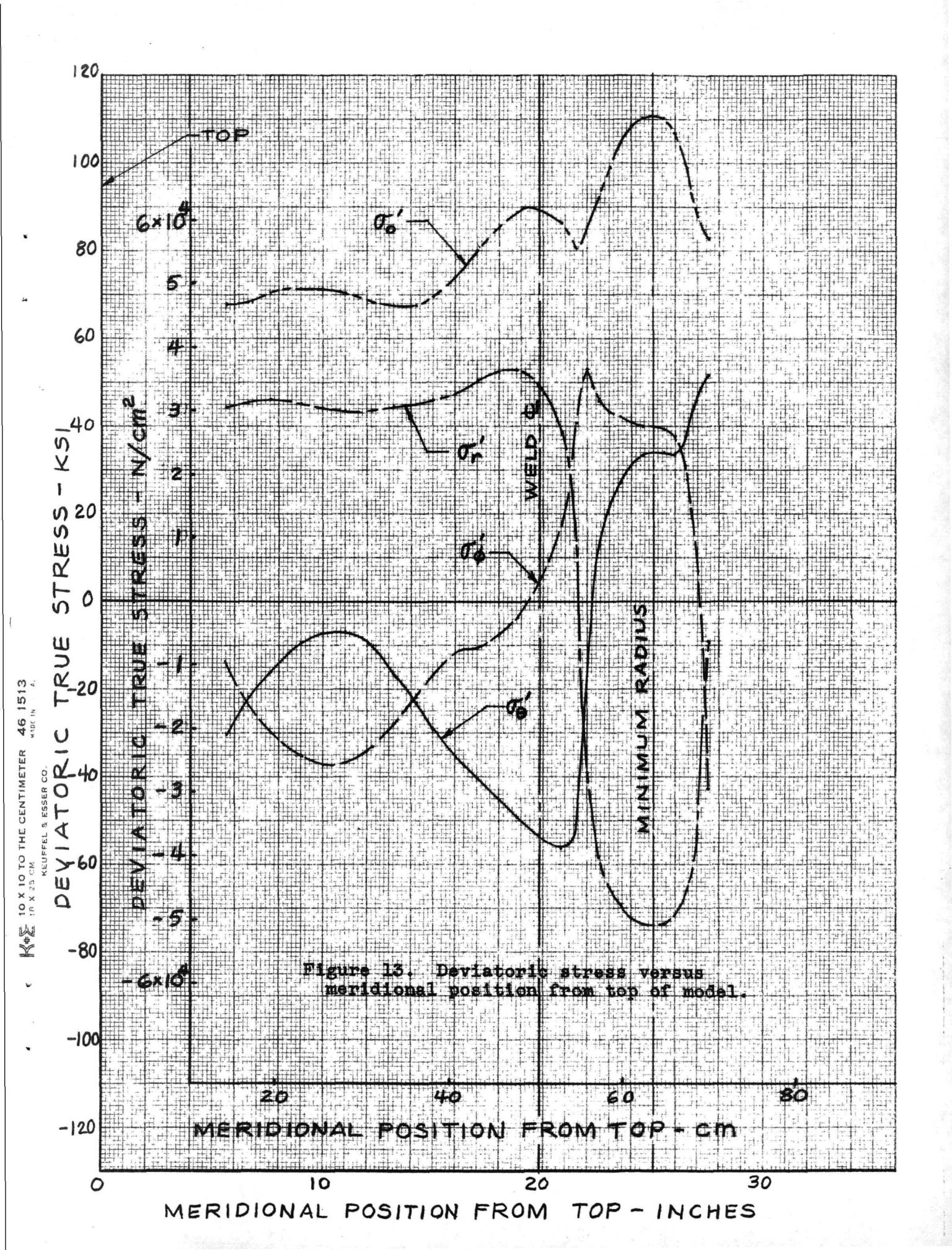

Figure 13. Deviatoric stress versus meridional position from top of model.

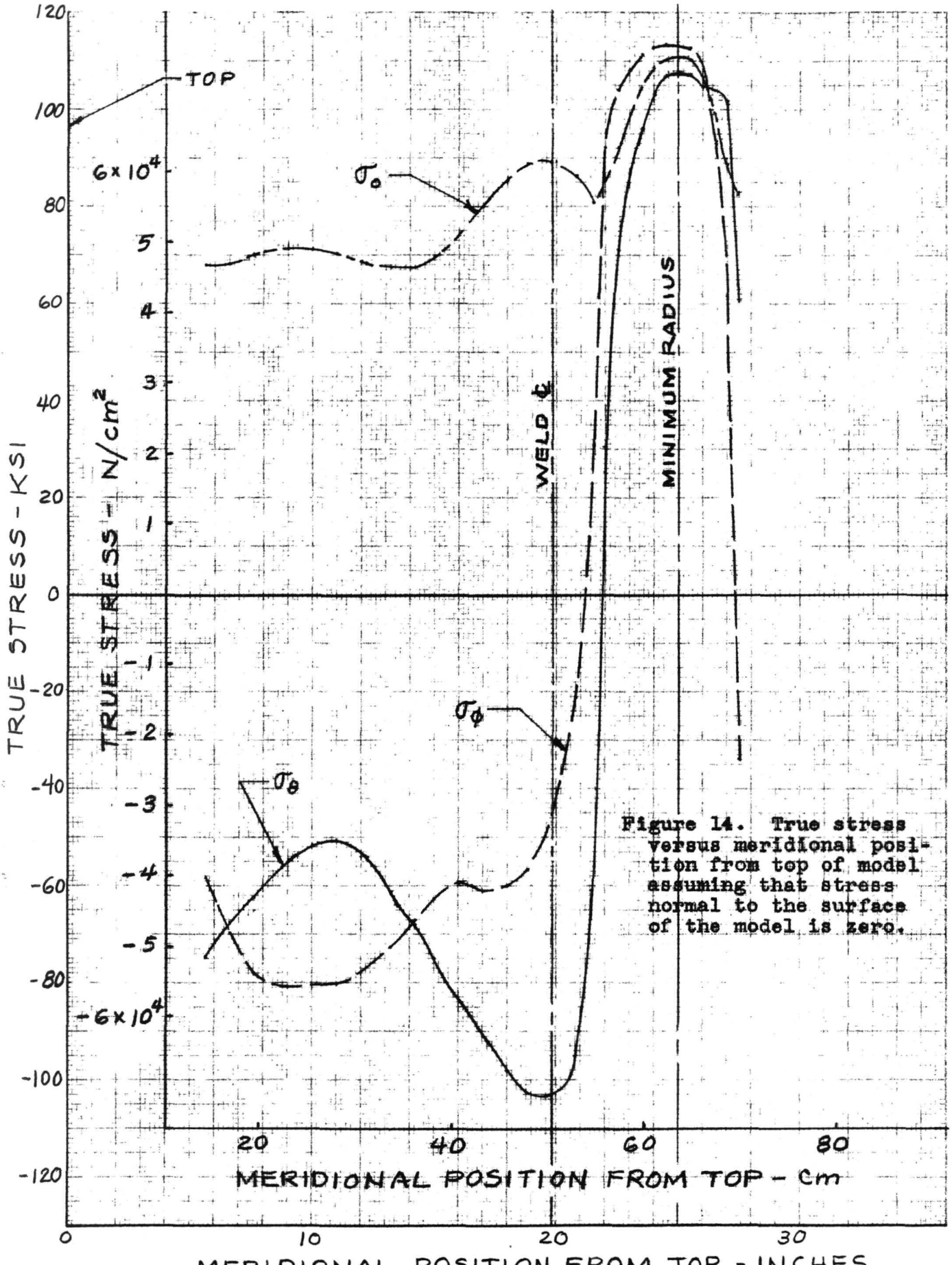

Figure 14. True stress versus meridional position from top of model assuming that stress normal to the surface of the model is zero.